High-spectral-resolution lidar with iodine-vapor filters: measurement of atmospheric-state and aerosol profiles

John W. Hair, Loren M. Caldwell, David A. Krueger, and Chiao-Yao She

A high-spectral-resolution lidar can measure vertical profiles of atmospheric temperature, pressure, the aerosol backscatter ratio, and the aerosol extinction coefficient simultaneously. We describe a system with these characteristics. The transmitter is a narrow-band (FWHM of the order of 74 MHz), injection-seeded, pulsed, double YAG laser at 532 nm. Iodine-vapor filters in the detection system spectrally separate the molecular and aerosol scattering and greatly reduce the latter (−41 dB). Operating at a selected frequency to take advantage of two neighboring lines in vapor filters, one can obtain a sensitivity of the measured signal-to-air temperature ratio equal to 0.42%/K. Using a relatively modest size transmitter and receiver system (laser power times telescope aperture equals 0.19 Wm^2), our measured temperature profiles (0.5–15 km) over 11 nights are in agreement with balloon soundings to within 2.0 K over an altitude range of 2–5 km. There is good agreement in the lapse rates, tropopause altitudes, and inversions. In principle, to invert the signal requires a known density at one altitude, but in practice it is convenient to also use a known temperature at that altitude. This is a scalable system for high spatial resolution of vertical temperature profiles in the troposphere and lower stratosphere, even in the presence of aerosols.

OCIS codes: 010.1280, 010.3640, 280.1100, 280.3640.

1. Introduction

After successful measurements of aerosol distribution in the troposphere with lidars, the need to measure aerosol and atmospheric parameters, such as temperature, was generally recognized. Fiocco *et al.*[1] demonstrated the feasibility of using a Fabry–Perot interferometer to reject aerosol scattering and of measuring temperature and the backscatter ratio in the troposphere by Cabannes–Mie scattering. Here, to be historically correct, we are reminded that Lord Rayleigh measured the scattered light consisting of a central peak, termed Cabannes scattering, and sidebands, termed (pure) rotational Raman scattering.[2] Because of the strict requirement in transmitter spectral purity, Fiocco *et al.* used a single-mode cw argon-ion laser, yielding such measurements without mentioning spatial resolution. Schwiesow and Lading[3] attempted to reject Mie scattering with a Michelson interferometer and to measure temperature profiles by Cabannes scattering without practical success. Temperature measurements by Rayleigh scattering, on the other hand, enjoyed an earlier success in the stratosphere and mesosphere where it is free from aerosol interference. In this case, a broadband laser is used to probe the profile of molecular density, from which atmospheric temperatures are calculated when local thermal and hydrostatic equilibrium are assumed. Elterman[4] demonstrated that such a data retrieval system is possible with a searchlight source, and he also observed seasonal dependence of atmospheric parameters.[5] Sanford later used a ruby laser to demonstrate similar measurement capabilities, and his data were shown in an early review paper by Kent and Wright.[6] Modern-day Rayleigh lidar, based on the same principles, that allows routine data acquisition was developed by Hauchecorne and Chanin.[7] Such a method, however, depends on an atmosphere free from aerosol contamination; it is therefore difficult for data retrieval below 30 km in altitude. With wide spectral separation from Rayleigh scattering, the vibrational Raman-scattering signal is free from aerosol contamination and can be used for temperature profiling based on the same data inversion technique[8] provided that there exists no sharp gradient in the extinction coefficient profile. This method, however, suffers 3 orders

When this research was performed, all the authors were with the Department of Physics, Colorado State University, Fort Collins, Colorado 80523. J. W. Hair is now with the NASA Langley Research Center, Mail Stop 401A, Hampton, Virginia 23681. The e-mail address for D. A. Krueger is Krueger@lamar.colostate.edu.

Received 17 October 2000; revised manuscript received 29 May 2001.

0003-6935/01/305280-15$15.00/0

of magnitude reduction in scattering efficiency. Rotational Raman scattering, which is ~2.5% efficient as compared with Cabannes scattering but requires a moderate laser spectral purity, has also been proposed[9] and applied[10–12] for temperature measurements. This technique still suffers from a weak signal and from the difficulty in the separation of rotational Raman scattering from the nearby Rayleigh–Mie scattering by means of interference filters.

Despite this difficulty in the spectral separation of aerosol scattering from molecular scattering, use of Cabannes scattering for the retrieval of atmospheric parameters, such as the backscatter ratio and temperature, is still attractive. By monitoring both transmission and reflection signals from a Fabry–Perot interferometer tuned to reflect most of the Mie scattering, the Wisconsin group was able to measure the profiles of the backscatter ratio successfully,[13] and they coined the name high-spectral-resolution lidar (HSRL). The problems encounted when molecular scattering is isolated completely from aerosol scattering with a Fabry–Perot makes temperature measurements difficult if not impossible. Use of a novel atomic or molecular filter[14] appears to be necessary if Cabannes scattering in the troposphere is to be monitored. Use of an iodine absorption cell later improved the backscatter ratio measurement considerably.[15]

Our own involvement in tropospheric temperature and other atmospheric parameter measurements was prompted by recognition of the difficulty in optical alignment and incomplete rejection of aerosol scattering using either Michelson or Fabry–Perot interferometers. We thus proposed use of an atomic vapor filter as a frequency discrimination[14] that can reject aerosol scattering in excess of 30 dB without the need of critical optical alignment for HSRL. With a barium filter, our group successfully measured the backscatter ratio profile soon after such a lidar system at 554 nm was installed.[15] The University of Wisconsin group succeeded in similar atmospheric measurements with an iodine filter.[16] Temperature profiling proved to be much more difficult. Implementation of a lead filter for HSRL by Voss *et al*.[17] unfortunately did not succeed for temperature measurements in the tropopause. Our implementation of a working HSRL based on an atomic or molecular filter proceeded in stages as described below.

We measured our first-stage temperature and backscatter ratios using two barium atomic vapor filters in the receiver and a pulsed-dye-amplified single-frequency dye laser tuned to 554 nm.[18] Although this system developed by Alvarez *et al*.[19] had temperature uncertainties as large as 10 K, the potential of a HSRL to measure atmospheric and aerosol parameters was fully demonstrated. There are several factors that led to a large temperature uncertainty. The main one is attributable to the fluctuations and lack of stability in the vapor filter transmission resulting from the high operating temperatures (~700–800 K) needed to provide the necessary barium density and sensitivity to air temperature. Other problems of secondary importance resulted from our having to tune the laser frequency manually to the barium transition without an automatic feedback locking mechanism, thus degrading the system stability. In addition, the detection of unwanted rotational Raman scattering degraded the measurement sensitivity. To improve temperature measurements compared with the barium system in our intermediate stage of development, Caldwell[20] developed a prototype system at 589 nm that used one iodine-vapor filter, which could be controlled at lower temperatures with better stability. He also employed Doppler-free spectroscopy to lock and tune the laser to the two preset iodine Doppler-free absorption lines[21] and inserted a Daystar Corporation filter with a 100-GHz bandwidth into the receiving system to reject the rotational Raman signal all together. With this system, Caldwell achieved a temperature accuracy better than 4.6 K at 1 km with a 375-m and 82-min resolution. The main uncertainty is due to a relatively small number of counts leading to poor photon-counting statistics. The low counts were the result of use of a photomultiplier that had relatively low maximum count rates for a linear response, which limited the amount of usable transmitted laser power to no more than 25 mW to avoid pulse pileup in the receiving system at the low altitudes. This gave rise to a temperature uncertainty that was due to photon noise of 3 K at 1 km, which dominates the measurement error, a problem that can be easily overcome. Unlike the barium system, the vapor filters did not limit the measurements.

Both the barium system at 554 nm and the iodine-vapor filter system at 589 nm were operated at wavelengths that required a dye oscillator and a pulsed dye amplifier to provide the narrow bandwidth necessary for temperature measurements. Although they are versatile, they are not appropriate for routine operation. Based on the iodine filter and the method of frequency locking developed, an all-solid-state transmitter operating at 532 nm was then implemented to provide a more robust and potentially transportable system for routine operation. The prototype working HSRL system is the topic of this paper.

2. High-Spectral-Resolution Lidar System at 532 nm

Because the lidar system uses the spectral information from the scattered returns and should be capable of tuning to an iodine absorption line, the laser transmitter must have high spectral resolution (~100 MHz) and be tunable over ~10 GHz. Such a lidar setup is shown in Fig. 1. The transmitter shown in Fig. 1(a) consists of a Lightwave Model 142 cw dual-wavelength laser having 50 mW of both 1064- and 532-nm light. The 1064-nm light is used to seed a pulsed Spectra-Physics YAG laser (Model DCR-3A) that is doubled to produce the transmitted laser beam and is frequency tunable with a near-Fourier-transform-limited line shape. The cw seed laser is

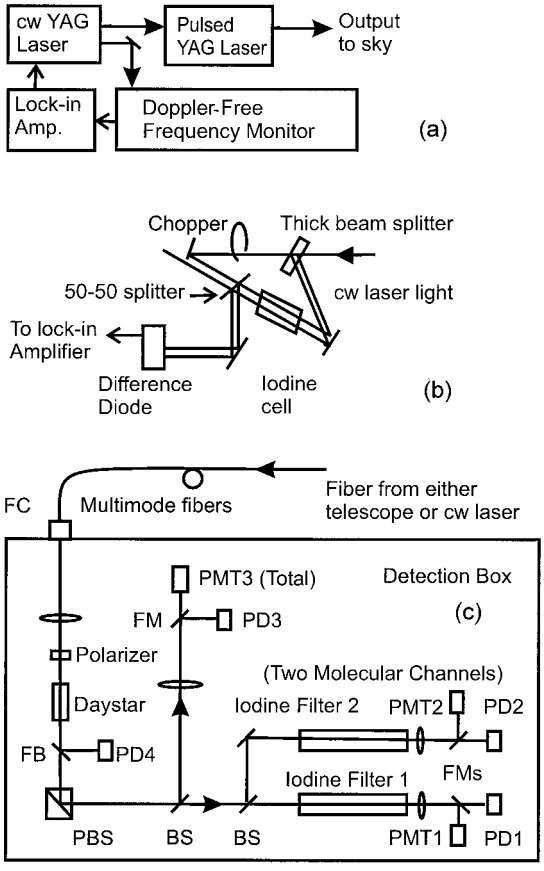

Fig. 1. Schematic of the HSRL system. (a) The transmitter system consists of a seeded, pulsed YAG laser of 74-MHz linewidth. (b) Details of the Doppler-free frequency monitor. (c) The receiver consists of two molecular and one total scattering channels. A schematic of the detection box is shown for the HSRL field measurements. The collected light is directed into a multimode fiber and then is input into the detection box where the light is passed through the Daystar Corporation filter and is then split into two channels that have iodine-vapor filters and one without a vapor filter. PBS, polarizing beam splitter; BS, dielectric plate beam splitter; FM, flip mirror; FB, flip beam splitter; PMT, photomultiplier tube; PD, photodiode; FC, fiber coupler.

frequency locked to an iodine Doppler-free saturated absorption line with the setup shown in Fig. 1(b),[22] with an active feedback control loop to provide an absolute frequency reference. In the Doppler-free technique only those iodine molecules in the laboratory cell with zero velocity along the laser beams will be on resonance with both of the counterpropagating laser beams and give rise to saturation effects that are not Doppler broadened and allow precise frequency control. Laser transmitter properties are summarized in Table 1.

The receiving system is shown in Fig. 1(c). Unlike the system at 589 nm that used one iodine filter and two transmitter frequencies, this system uses two iodine filters and one transmitter frequency because the frequency of the YAG laser cannot be rapidly tuned. The filters are different because they are maintained at different temperatures. The lidar system measures the temperature and aerosol profiles in the troposphere, thus requiring the system to handle a large dynamic range in the collected signal. The new lidar system improves the maximum linear count rates to utilize all 6 W of laser power that is available, which is considerably higher than the 25 mW used in the 589-nm system. Compared with the 589-nm system,[20] more than ten times the linear photocount rate was received without saturation, allowing the photon-counting errors to be significantly reduced. New photomultiplier tubes (PMTs) that have a higher maximum linear count rate, along with a biaxial transmitted beam 20 cm from the receiving telescope axis to change the geometric overlap at small ranges, were incorporated to reduce the counts at lower altitudes and still provide the maximum possible counts in higher altitudes.

Table 1. System Parameters for Transmitter and Receiver

Transmitter and Receiver	Parameter
Spectra-Physics Pulsed YAG	
Laser Model DCR-3A	
Average power	6 W at 532 nm
Pulse duration	5 ns
Divergence	0.5-mrad full angle
Pulse repetition rate	20 Hz
Linewidth (FWHM)	74 MHz
cw Light-wave Model 142	
Average power	50 mW at 532 nm, 50 mW at 1064 mW
Linewidth	$<$10 kHz
Tuning range	$>$10 GHz
Locking accuracy	2 MHz
Detection System	
Telescope	0.203-m-diameter Cassegrain
Photomultiplier tubes	H5783P Hamamatsu
Iodine filters (57 °C, 82 °C) (full widths)	3.0 GHz, 4.3 GHz
Daystar Corporation filter	1.3 Å FWHM
Counting board interface	Optech 700-MHz multichannel scalar average

The detection system uses a relatively small 0.203-m Cassegrain telescope pointing to zenith, giving a power-aperture product of 0.19 Wm^2. The light is coupled with a lens into a 365-μm multimode fiber with a N.A. of 0.22. The fiber output is sent into the detection box shown in Fig. 1(c). The lens and fiber were selected to satisfy several constraints. The first is to collimate the output of the fiber over ~1 m along the beam with a beam diameter of ~25 mm. This yields a reasonable beam collimation to pass through the Daystar Corporation filter, polarizing elements, and the iodine filters. The Daystar Corporation filter eliminates rotational and vibrational Raman-scattered light from the return signal, avoiding the need to include them in data analysis. This filter is broad enough to pass almost all the Cabannes–Mie signal. In addition, this narrower bandwidth also allows measurements to be made at dusk and dawn. The signal is then split into three channels. Two molecular-scattering channels have iodine-vapor filters, along with an unfiltered channel

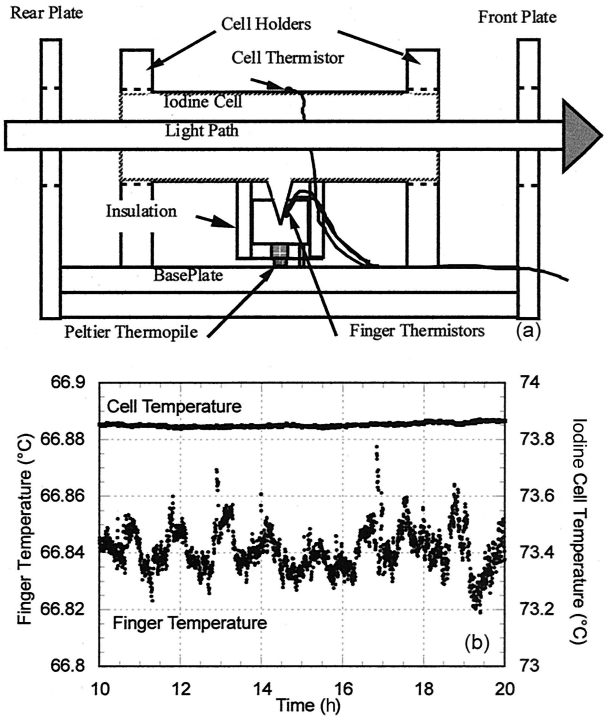

Fig. 2. (a) Detailed drawing of the iodine-vapor filter oven without the external housing. (b) Iodine cell finger and iodine cell temperatures as a function of time. The data presented here were taken every 15 s over a 10-hr period.

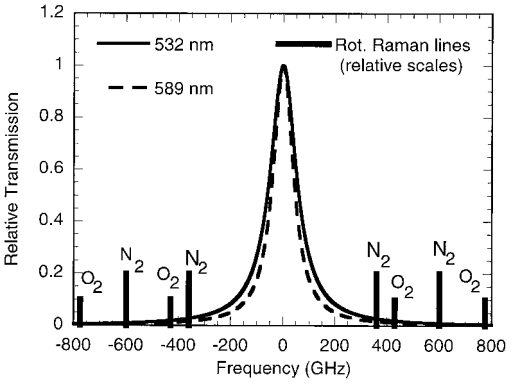

Fig. 3. Normalized bandpass transmission curves for the Daystar Corporation filters operated near 532 and 589 nm. The first few pure rotational Raman lines are plotted; they are effectively blocked.

that measures the total Cabannes–Mie scattering as shown in Fig. 1(c). Figure 2(a) shows a schematic of the iodine cell. Because we have equilibrium between iodine vapor and solid, the vapor pressure is determined by the temperature of the cooler finger where the solid resides. This pressure, along with the cell temperature, determines the density of vapor in the cell. Because the vapor pressure is a sensitive function of the finger temperature, it is imperative to control the finger temperature accurately. Figure 2(b) shows that the temperatures of the cell and the cooler finger are stable over several hours. The iodine filter transmission functions were measured as a function of frequency and characterized for the lidar inversion and are discussed in Section 3. The two iodine filters, operated at cell temperatures of 82 °C and 57 °C, have a different transmission as a function of frequency, yielding two independently filtered molecular-scattering signals. Even though the filters have complicated spectra, the extinction at line center is greater than 34 dB for a filter width of ~2 GHz, in the same order as the Cabannes-scattering spectral width. The laser frequency was locked[22] to a Doppler-free feature in the 1108 iodine absorption line.

3. Principle and Practice of the High-Spectral-Resolution Lidar Measurements at 532 nm

In response to a narrow-band single-frequency laser beam, the backscattered light from the atmosphere is composed of several components: Cabannes, rotational and vibrational Raman scattering from the air molecules, and aerosol (Mie) scattering. Because the aerosols are much more massive than the molecules, the spectral broadening of the Mie scattering (~10 MHz) is much smaller than the Cabannes scattering (width ~2 GHz). The rotational Raman-scattering spectrum is separated from the laser frequency by more than 150 GHz and is filtered by a narrow-bandpass Daystar Corporation filter (130 GHz FWHM) as shown in Fig. 3 and therefore is not considered in the equations below.

The detected photocounts at a range z in the total scattering channel N_t and the molecular-scattering channels $N_{m,i}$, where i (=1 or 2), are given in Eqs. (1a) and (1b) in terms of the normalized Daystar transmission function $D(\nu)$ and the normalized Cabannes–Brillouin function $\Re(\nu, T, P)$:

$$N_t = (E_0/h\nu)(A/z^2)\Delta z\xi_t[\beta_a(z) + \beta_m(z) f_D]\exp\left[-2\int \mathrm{d}z'\alpha(z')\right], \quad (1a)$$

$$N_i = (E_0/h\nu)(A/z^2)\Delta z\xi_m[\beta_m(z) f_i] \times \exp\left[-2\int \mathrm{d}z'\alpha(z')\right], \quad (1b)$$

$$f_D(T, P) = \int \Re(\nu, T, P) D(\nu)\mathrm{d}\nu, \quad (1c)$$

$$f_{m,i}(T, P) = \int \Re(\nu, T, P) F_i(\nu) D(\nu)\mathrm{d}\nu, \quad (1d)$$

where

$$\int \Re(\nu, T, P)\mathrm{d}\nu = 1. \quad (1e)$$

Here, f_D and $f_{m,i}$ in Eqs. (1c) and (1d) are attenuation factors of Cabannes scattering[23] by, respectively, the

normalized Daystar function and the combination of the normalized Daystar and the normalized iodine transmission filter. In Eqs. (1a) and (1b), E_0 is the energy of laser pulses summed over the integration time duration; and ξ_t, ξ_i are the efficiency factors of the three channels [Fig. 1(c)], including the telescope overlap function [which is unity for the ranges of interest (>100 m)], the splitting, collection, and detection. It should be noted that the geometric overlap function is the same for all three channels. Because different iodine filters were used for the two molecular channels, ξ_1 and ξ_2 are different. A is the area of the receiving telescope, h is Planck's constant, and ν is the laser frequency. The total volume backscatter coefficient is $\beta = \beta_a + \beta_m$, the sum of aerosol and molecular contributions. The Raman scattering is blocked by a Daystar Corporation filter with transmission function $D(\nu)$, allowing $f_{m,i}(T, P)$ to be calculated[24] from laboratory-measured transmission functions of the iodine and Daystar Corporation filters $F_i(\nu)$ and $D(\nu)$, respectively, as well as the normalized Cabannes–Brillouin-scattering function[25] $\Re(\nu, T, P)$. We normalized the functions $D(\nu)$ and $F_i(\nu)$ by setting to unity the peak transmission of $D(\nu)$ and the peak transmission with the iodine filter removed. Here, the normalized $\Re(\nu, T, P)$ is a Cabannes–Brillouin-scattering function that we calculated based on the S6 theoretical model of Tenti *et al.*[26] The actual filter transmissions, which depend on the frequency-independent efficiency factors ξ_i, are determined experimentally as discussed in Subsection 3.B.

To obtain the atmospheric temperature we assume that the pressure at a starting range height is known. Then the temperature follows from the ratio of the received photon counts of the two molecular channels:

$$N_1/N_2 = \xi_1 f_{m,1}(T, P)/\xi_2 f_{m,2}(T, P). \quad (2)$$

When the pressure and temperature at one altitude along with equations of hydrostatic equilibrium and ideal gas law are known, then the pressure at the next range bin is obtained. Repeating this, we obtain the vertical profiles of pressure $P(z)$, density $n(z)$, and temperature $T(z)$.

With the atmospheric-state parameters derived, we can determine the total extinction coefficient $\alpha(z)$ by taking the spatial derivative of the signal from either molecular channel:

$$\alpha(z) = 0.5\mathrm{d}[\beta_m \xi_i f_{m,i}(T, P)/(N_i z^2)]/\mathrm{d}z. \quad (3)$$

Given f_D and $f_{m,i}$, the backscatter ratio $[\beta_a(z) + \beta_m(z)]/[\beta_m(z)]$ can be determined from the ratio of the total scattering channel and one of the molecular channels as

$$N_t/N_i = (\xi_t/\xi_i)[\beta_a(z) + \beta_m(z) f_D]/[\beta_m(z) f_{m,i}]. \quad (4)$$

All the self-consistent results of Eqs. (2)–(4) depend on our ability to measure ξ_t/ξ_i and ξ_1/ξ_2 as well as the normalized filter functions $D(\nu)$, $F_1(\nu)$, and $F_2(\nu)$. Fortunately, with a fiber coupler used in the detection portion, we can perform the necessary measurements using essentially the same setup without disturbing the alignment or altering the operational conditions of the detector box. To determine the necessary quantities, we perform two sets of laboratory experiments as follows.

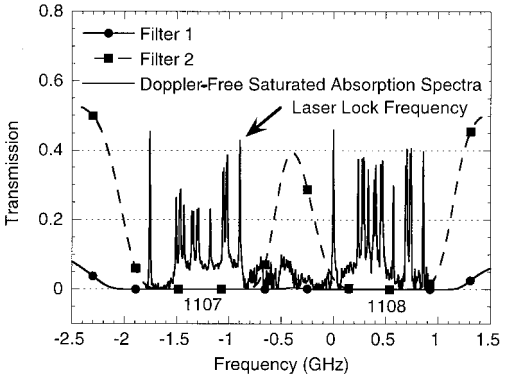

Fig. 4. Iodine transmission curves for filters 1 and 2 that have cell (finger) temperatures of 82.19 (72.03) °C and 56.18 (47.74) °C, respectively. Also plotted is the Doppler-free spectrum for lines 1107 and 1108. The laser locking is marked for reference.

A. Measurement of $D(\nu)$ and Relative Functions $S_i(\nu)$

For the measurements of the normalized Daystar transmission function $D(\nu)$ and the relative functions of the $F_i(\nu)D(\nu)$ product or $S_i(\nu)$ for two molecular channels, which may be performed on a day different from the atmospheric observation, we replace the three PMTs by three photodiodes by means of flip mirrors. A fourth flip mirror and diode are added to normalize out the laser intensity fluctuations. We then send a highly attenuated cw seed beam into the receiving fiber. A scan of the cw seed laser over a frequency range in excess of 10 GHz allows us to determine these functions from the signal of the photodetectors $I_1(\nu)$ through $I_4(\nu)$ as follows:

$$D(\nu) = \xi' I_3(\nu)/I_4(\nu), \quad (5)$$
$$S_i(\nu) = \xi'_i F_i(\nu) D(\nu) = I_i(\nu)/I_4(\nu),$$

with $i = 1$ or 2. Here ξ' is a constant that is needed to scale the peak transmission of $D(\nu)$ to unity. The measured normalized transmission function of the Daystar Corporation filter for 589 nm and the estimated transmission for 532 nm are shown in Fig. 3. The constant factors ξ_i', which depend on the efficiency of the photodiodes, are unknown. Because the normalized Daystar function is nearly unity within ±5 GHz near its peak, the measured $S_i(\nu)$ can be regarded as the relative transmission functions of the iodine filter $F_i(\nu)$ at operational temperatures. These measured functions are shown in Fig. 4 along with the simultaneously measured Doppler-free spec-

trum.[25] With the measured function $S_i(\nu)$, we can evaluate the effective attenuation factors

$$f_i^S(T, P) = \int \Re(\nu, T, P) S_i(\nu) D(\nu) \mathrm{d}\nu = \xi_i' f_{m,i}(T, P), \tag{6}$$

where $S_i(\nu) = \xi_i' F_i(\nu) D(\nu)$ and relate the effective attenuation factors defined in Eqs. (5) to the attenuation factor defined in Eq. (1d); $f_i^S(T, P) = \xi_i' f_{m,i}(T, P)$ as indicated in Eq. (6). In terms of the effective attenuation factors, $f_i^S(T, P) = \xi_i' f_{m,i}(T, P)$; Eqs. (2)–(4) for the atmospheric parameter retrieval are finally replaced by

$$N_1/N_2 = (\xi_1\xi_2'/\xi_2\xi_1')[f_1^S(T, P)/f_2^S(T, P)], \tag{7}$$

$$\alpha(z) = 0.5\mathrm{d}[\beta_m(z)\xi_i f_i^S(T, P)/(\xi_i' N_i z^2)]/\mathrm{d}z, \tag{8}$$

$$N_t/N_i = (\xi_i'\xi_t/\xi_i)[\beta_\alpha(z) + \beta_m(z) f_D]/[\beta_m(z) f_i^S(T, P)]. \tag{9}$$

Because of the spatial derivative, the unknown factor ξ_i' will not affect the result of Eq. (8). However, to use Eqs. (7) and (9) for the retrieval of atmospheric temperatures and the backscatter ratio, respectively, the combinations $(\xi_1\xi_2'/\xi_2\xi_1')$ and $(\xi_t\xi_i'/\xi_i)$ must be determined by laboratory experiments. Note that, because $D(\nu)$ can be scaled to unity, the attenuation factor f_D is set to unity hereafter.

B. Normalization Measurements for $(\xi_1\xi_2'/\xi_2\xi_1')$ and $(\xi_t\xi_i'/\xi_i)$

To determine the required combinations of $(\xi_1\xi_2'/\xi_2\xi_1')$ and $(\xi_t\xi_i'/\xi_i)$, we flip out all the diode channels and restore the PMTs in the three channels. The detection box is now identical to that used for field measurement. We then use the highly attenuated cw seed laser light as before and tune the laser off resonance to a flat part of the filter function at ν_0 just outside the range shown in Fig. 4. The mean values as measured by the three PMTs in the two molecular channels N_1 and N_2 and the total scattering channel N_t can be used to express the desired parameters $(\xi_1\xi_2'/\xi_2\xi_1')$ and $(\xi_t\xi_i'/\xi_i)$ in terms of the measured normalization ratios $(N_1/N_2)_{\mathrm{NORM}}$ and $(N_t/N_i)_{\mathrm{NORM}}$. We can then express Eqs. (7) and (9) in terms of these measured normalization ratios and the known $S_i(\nu)$ at ν_0 as shown in Eqs. (10) and (11):

$$(N_1/N_2)_{\mathrm{NORM}} = \xi_1\xi_2' S_1(\nu_0)/\xi_2\xi_1' S_2(\nu_0),$$
$$N_1/N_2 = (N_1/N_2)_{\mathrm{NORM}} S_2(\nu_0) f_1^S(T, P)/S_1(\nu_0) f_2^S(T, P), \tag{10}$$

$$(N_i/N_i)_{\mathrm{NORM}} = \xi_T\xi_i'/\xi_i S_i(\nu_0),$$
$$(\beta_m + \beta_\alpha)/\beta_m = (N_t/N_i)(N_i/N_t)_{\mathrm{NORM}} f_i^S(T, P)/S_i(\nu_0). \tag{11}$$

In Eq. (11) we set the Daystar attenuation factor f_D to unity as explained above. Unlike the relative functions $S_i(\nu)$, whose stability can be monitored by the cell and finger temperature of the iodine filter and the Daystar Corporation filter, the normalization measurements must be performed before or after the field measurement as the overall efficiency of the different channels may vary from one day to the next. This could include the changes of the frequency-independent continuum absorption that is due to small fluctuations in the temperature. The continuum absorption is much more sensitive to temperature changes in the filters than the frequency-dependent absorption of iodine.[26] Fortunately, when we use a fiber coupler, it facilitates the normalization measurement to be performed without perturbing the alignment of the detector box.

4. Temperature Measurement Sensitivity of Square-Well and Iodine-Vapor Filters

To aid in understanding the performance of real filters, we first discuss an ideal square-notch filter. This ideal filter has zero transmission centered on the laser frequency over a filter width that can be varied and has 100% transmission at other frequencies. The shape of the notch filters that are used influences the accuracy of atmospheric temperatures determined when we use the HSRL technique. For real filters the transmission within the filter absorption band determines the rejection of the collected aerosol scattering by the filters. The width and slope of the filter absorption bands affect the sensitivity to air temperature changes and the fraction of the total Cabannes scattering that is transmitted through the filter. Rejection of aerosol scattering, sensitivity of the measured signal-to-air temperature ratio, and the fraction of the Cabannes–Brillouin-scattered light that passes the filter are thus the key factors for consideration; a proper balance between these is required for filters to be used for lidar application. The ideal filters give quantitative estimates of the air temperature sensitivity that estimates the performance of the iodine-vapor filters used in the HSRL. A characterization of the iodine-vapor filters used in the HSRL system operated near 532 nm follows.

A. Ideal Vapor Filters and Air Temperature Sensitivity

To understand the performance of different lidar systems, we turn our attention to the sensitivity of the measurement in response to changes of a 1-deg air temperature change for an atmosphere at a given atmospheric temperature T_0 and pressure P_0. The single-channel sensitivity $\Delta N_i/N_i$ is defined as the fractional change in the Cabannes–Brillouin-scattering signal passing through an ideal filter of a given width. We use the theoretical model of Tenti *et al.*[26] for Cabannes–Brillouin spectra. The air temperature measurement sensitivity S_T is the difference in this fractional change for the two filters used:

$$S_T = S_{T_1} - S_{T_2} = \Delta N_1/N_1 - \Delta N_2/N_2. \tag{12}$$

The maximum sensitivity that an ideal square filter can produce is expected to be an upper limit for

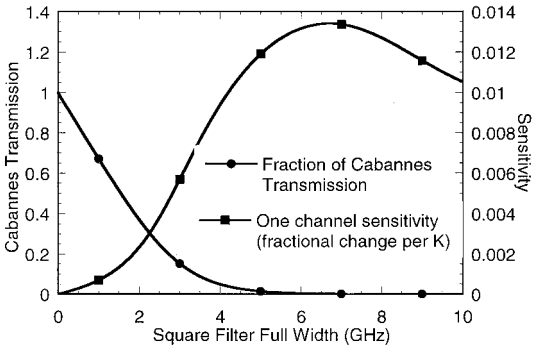

Fig. 5. One-channel sensitivity in percent change in the lidar signal for a 1 K change in the air temperature and the fraction of the Cabannes–Brillouin signal ($T = 275$ K and $P = 0.75$ atm at 532 nm) transmitted through an ideal square filter as a function of the filter full width.

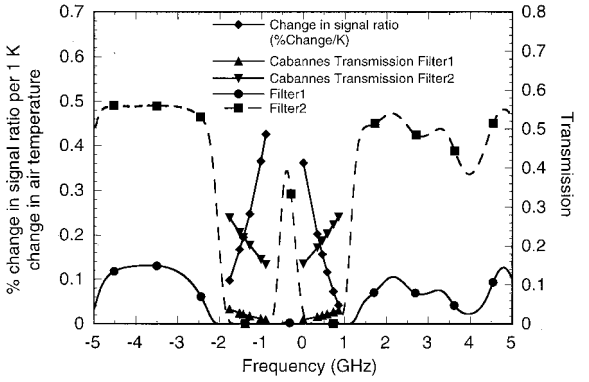

Fig. 6. Measured iodine filter transmission curves near 532 nm. The fractional change in the signal ratio and the fraction of the Cabannes signal pass through the filters at selected frequencies for scattering calculated at $T = 275$ K and $P = 0.75$ atm. The two absorption bands overlap to give an effectively larger filter width for use in the HSRL.

any physical filter used in the HSRL. Figure 5 shows the percent change in the molecular signal for a 1 K change in air temperature ($\Delta N_i/N_i$) as a function of the full width of an ideal filter. The fraction of the Cabannes signal that passes through the filter is also plotted for comparison. The maximum fractional change for an individual filter is near 1.3%/K for a square filter of full width ~7.0 GHz, suggesting that the upper limit to S_T is 1.3%/K. The fraction of the Cabannes signal that passes through the filter is small (<0.1%) for a filter width of 7.0 GHz and would not be practical. To have 1% of the Cabannes signal pass the filter, the filter width must be less than 5 GHz. Because the measurement requires the aerosol scattering to be mostly filtered, the narrower filter cannot be zero. A filter width of ~200 MHz is the minimum that would be necessary to eliminate the aerosol scattering. This width is twice the laser line-shape width for the transmitter used in this lidar system.

With these restrictions on the width and signal strengths, one would use two ideal square-notch filters with widths of 0.2 and 5 GHz that give sensitivities to air temperature of 1.1%/K, with 93% and 1% of the Cabannes-scattered light passing through the filters, respectively. For comparison, consider the barium-vapor filters; the sensitivity of the molecular signal-to-air temperature ratio for barium filters for several different full widths was reported by Krueger *et al.*[24] The sensitivity of the ratio for the 1.7- and 3.3-GHz barium filters is 0.26%/K. This compares with 0.6% for the ideal filters shown in Fig. 5. The barium transmissions are close to ideal for a practical filter. Therefore, to further increase the sensitivity by use of iodine filters, the filter width would need to be increased further. The sensitivity to air temperature was 0.24%/K for the system developed at 589 nm by use of iodine filters[20] operated in a pair of overlapping lines. For measurements made from ground to 10 km with a signal dynamical range of 5 orders of magnitude, it is difficult to have good temperature accuracy over the entire height range with sensitivities smaller than 0.2%/K for HSRL at 532 nm and with a small power-aperture product of ~0.19 Wm^2 in our case.

B. Iodine Filters

Because molecular iodine has many strong absorption lines over the visible spectrum that are experimentally detectable even with low cell temperatures (60 °C–80 °C) compared with barium filters (950 °C), an iodine filter could be temperature controlled more easily. This was proven to work for temperature and aerosol measurements at 589 nm in a two-frequency single-iodine-channel setup.[25] In addition, with many absorption lines near 532 nm, iodine gives several options for locking frequencies within the tuning range of commercially available solid-state seed lasers, from which one can select an operational frequency for high measurement sensitivity.

Because the temperature measurement requires that the aerosol scattering be almost completely filtered from the return signal, and with the laser lock frequency (marked in Fig. 4) chosen to be near the center of the overlapping absorption of lines 1107 and 1108 to take the advantage of high temperature measurement sensitivity, the lowest temperature for the cooler iodine cell should be near 60 °C for a 15.24-cm-long cell. Detailed study on various combinations of filter cell and finger temperatures were made[25]; it was concluded that, to obtain sensitivities to air temperature that are better than 0.2%/K, the hotter cell needed to be operated near 70 °C–80 °C.

The filter transmissions that are selected for lidar operation are plotted in Fig. 6. The cell length is 15.24 cm and the cell (finger) temperatures are 82.19 °C (72.03 °C) and 56.18 °C (47.74 °C) for hot cell (filter 1) and colder cell (filter 2), respectively. Also shown in Fig. 6 are the measurement sensitivities, i.e., the fractional change in the signal ratio per 1 K change in atmospheric temperature at different possible locking frequencies and the fraction of the molecular Cabannes signal passing through the filter (triangles). It is clear from these plots that the sig-

nal through the filters decreases as the sensitivity to air temperature measurement increases. Thus a balance is made between these two factors when we choose an operation frequency of the lidar.

The selection of the iodine filters was made from a selected range of frequencies that were accessible with the Lightwave 142 laser. This particular range of 10 GHz near 18,787.322 cm^{-1}, plotted in Figs. 4 and 6, is special in that there are two absorption bands (1107, 1108) that overlap. This allows the filter width of the hotter filter to be nearly twice as wide as a single absorption line. This turns out to be significant when we consider that it is difficult to obtain a single line that is more than ~2 GHz in width without going to a much higher cell temperature. Although, in principle, one can increase the bandwidth of an ideal filter by going to a higher temperature without changing the filter transmission at off-resonance frequencies, unfortunately this is not the case with the iodine filter. As can be seen from Figs. 4 and 6, the transmission at the off-resonance frequency, such as ν_0, is much lower (0.14) in the hotter filter than in the colder one (0.54). Increasing the cell temperature to obtain larger filter widths would result in an exponential increase in the continuum absorption and excessive loss of the Cabannes-scattering signal. Studies of continuum absorption in iodine have been made by Tellinghuisen[27] and Forkey[28] and its impact on lidar signals has been studied by Hair,[25] so we do not discuss this here. It is sufficient to note that the width of the notch filter affects the sensitivity of the measured ratio to air temperature change. The width for the colder cell should be selected as small as possible yet still have good rejection of the aerosols. We settled on 56 °C for the cold cell for our HSRL. Because of continuum absorption, we settled on a hotter cell filter width at ~82 °C that achieved 0.42% measurement sensitivity and still passes at least 1% of the Cabannes-scattered signal. The aerosol-scattering rejection is determined from the transmission of the iodine filters within the absorption line. At the laser lock frequency, we measured aerosol rejection of −41 and −48dB, respectively, for the cold and hot filters.

5. Results of Field Measurements

Eleven nights of data were taken between January and June 1998 at Christman Field, Fort Collins, Colorado (40.6 °N, 105 °W, 1569 m above sea level). Most of the data taken were in the evening hours, with some nights running past sunrise into the early morning hours. Most of the data can be compared with local Denver and Fort Collins balloon soundings to assess the temperature measurement accuracy and precision of our working HSRL.

Table 2 gives a list of nights that the HSRL data were taken. The filter transmission curves were taken periodically to ensure that they remained the same. Any time the filter cell temperatures changed, new transmission curves were measured. All nights used three channels of data, allowing calculations of both the state parameters and the backscatter ratios. All lidar raw data profiles collected were initially summed over 3-min intervals and have a 75-m range resolution. Data were later processed at different averaging times and range resolutions. Also given is the duration of the data set. For all nights there were two sets of balloon data from Denver for comparison. For the night of 14 May 1998, there were also two sets of Fort Collins balloon data taken at Christman Field in support of these measurements. There were two balloons launched in Fort Collins: one on 19 June and one on 20 June. Compared with the balloonsonde, there is a temperature bias in the lidar data that we discuss in Subsection 5.B. The temperature offset, which can be as much as ~10 K, could be positive or negative, which is also given in Table 2. The offset percentage is approximately 0.41 times the temperature offset in degrees Kelvin. The relative efficiency problem also exists between the molecular and the total scattering channels. Because most nights had fairly clear weather, we estimate the backscatter ratio offset (as shown in the last column of Table 2) by assuming unity backscatter ratio at a range height where the backscatter ratio is minimum.

Table 2. Summary of the 1998 HSRL Lidar Measurements

Date (UT)	Time (UT)	Temperature Offset (K)[a]	Backscatter Ratio Offset (%)
14 January	5:55–10:32	+7	−5
15 January	2:30–11:05	+12	0
7 February	3:07–4:22	+10	−2
12 February	1:07–14:11	+6	−5
1 April	3:08–14:11	0	+5
11 April	2:07–10:17	−9	0
19 April	3:17–10:42	0	−5
30 April	2:28–8:28	+9	−5
14 May	2:39–11:31	+2	<1
19 June	4:17–10:32	−10	+<1
20 June	2:48–9:53	−7	+5

[a]Temperature offset was determined by comparison of lidar results with two Denver balloonsondes daily and two balloonsondes on 14 May, and one sonde on 19 June and one on 20 June launched from Fort Collins for the HSRL experiments.

A. Mean-Temperature and Backscatter Ratio Profiles

Following the data acquisition and analysis procedure outlined in Section 3, including the laboratory normalization measurements, the temperature profile measured by the HSRL still exhibits an offset between −10 and +12 K when compared with the balloon-sounding results. A multiplicative adjustment on relative efficiencies between the two molecular channels must be made for its correction. That such an offset exists can be seen in Fig. 7(a), where a 5-hr, 300-m averaged temperature profile measured on 19 June 1998 is shown. The fact the lidar temperature profiles with and without adjustment are nearly parallel to one another suggests that only one adjusting constant is needed. Indeed, we can determine the multiplicative factor by matching the lidar temperature and the balloon temperature at one

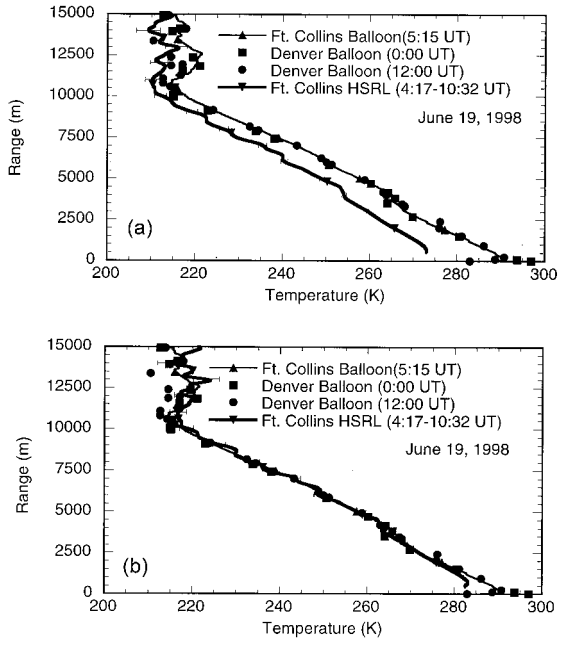

Fig. 7. HSRL 5-hr, 300-m averaged temperature profile for 19 June, 1998 plotted with the Fort Collins and Denver balloonsondes. The error bars give the effect of photon-counting statistical variations at selected heights for the HSRL data. (a) Lidar temperature profile is offset from balloon sounding. (b) With an adjustment factor as discussed in the text.

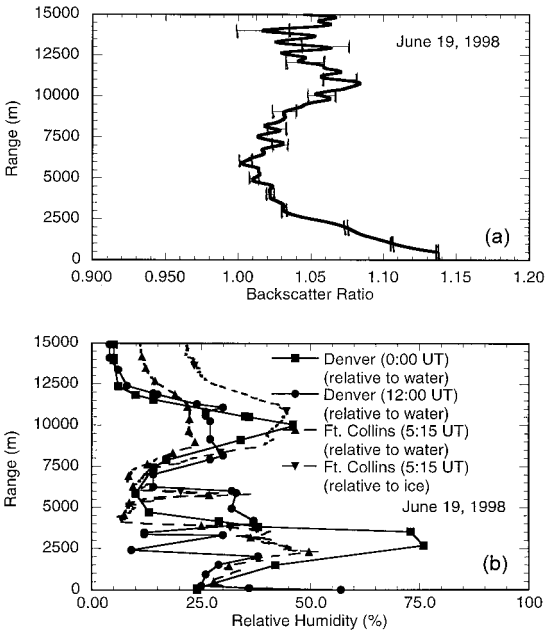

Fig. 8. (a) HSRL 5-hr, 300-m averaged backscatter ratio profile for 19 June, 1998 plotted with photon-counting error bars at 1-km intervals. (b) The relative humidity from the Fort Collins and Denver balloons is plotted for comparison with the HSRL backscatter ratio. A persistent peak in the relative humidity can be seen at ~10 km.

range height. Use of this factor so determined will make the two profiles fall on top of one another within the statistical experimental error bars as shown in Fig. 7(b). Both Denver and Fort Collins balloon data are plotted for comparison. On this night, both Denver balloons (at 0 UT and 12 UT) and the Fort Collins balloonsonde, which was launched about 1 hr after the lidar data were initiated, were in good agreement within the lidar photon noise uncertainty. Because the lidar temperature profile is parallel to balloon soundings below 8 km, we can make an offset adjustment by matching the lidar temperature to the balloon sounding at any range bin. Independent of the offset, as shown in Fig. 7(a), the lapse rates of the balloon and HSRL data match well. The measured lapse rates between 5 and 10 km are 8.0 and 7.9 K/km for the Fort Collins balloon and the HSRL, respectively. The lapse rate and tropopause altitudes are in agreement despite an offset, which is true for all nights we have data, suggesting that our lidar is a working system for HSRL measurements.

Figure 8(a) shows the 5-hr average of the backscatter ratio for 19 June, 1998. The error bars represent uncertainties that are due to the photon-counting noise at different altitudes. The average backscatter ratio peaks lower in the troposphere with 15% aerosol backscatter and peaks again at 10 km with ~7% over the pure air value. According to Table 2, the offset in the backscatter value is minimal on this night. Because this backscatter ratio profile is a bit atypical compared with other nights because of an increase at ~10 km, a plot of the relative humidity from balloon sounding, showing a persistent layer of water vapor at this height, is shown in Fig. 8(b), suggesting correlation between the lidar-measured backscatter ratio and the balloon-measured relative humidity. The amount of water vapor normalized to the ice-vapor-saturated vapor pressure curve is also plotted in Fig. 8(b); a better resemblance between the ice-vapor-based relative humidity profile and the lidar-measured backscatter profile is evident. At these temperatures (~217 K) in the tropopause region, ice particles are likely to be present.

B. Summary of Temperature Errors

The temperature calibration and measurement errors are summarized in Tables 3 and 4, respectively. The calibration errors include uncertainties in normalization measurement, filter transmission measurement, laser spectral purity, and reference

Table 3. Summary of Temperature Calibration Errors[a]

Source	Estimate	Percent Error in Temperature Ratio	Air Temperature Error (0.42%/K)
Normalization	0.7%	0.7	1.7
Frequency drift	<200 MHz	0.15	0.4
Filter transmission	0.95%	0.95	2.3
Laser spectral purity	<1%	1.0	5.0
Reference pressure	<15%	<0.12	0.3

[a]Total offset in worst case (added in magnitudes) is 9.7 K. Total offset for independent errors (added in quadrature) is 5.8 K.

Table 4. Summary of Temperature Measurement Errors[a]

Source	Estimate	Percent Error in Temperature Ratio	Air Temperature Error (0.42%/K)
Frequency lock stability	2 MHz	0.26	0.6
Iodine filter transmission stability	<0.18%	0.18	0.43
PMT stability	<0.71%	0.71	1.7
Photon noise at different ranges for 1-hr and 300-m integration	at 1 km	0.1	0.25
	at 2 km	0.2	0.51
	at 5 km	0.65	1.6
	at 10 km	1.5	3.7

[a]Total error (added in quadrature assuming sources of errors are independent): 1.9 K at 1 km, 1.9 K at 2 km, 2.4 K at 5 km, 4.1 K at 10 km.

pressure as well as frequency drift from the perceived laser locking point. The estimates of these uncertainties have been discussed in detail,[26] and their results are summarized in Table 3. Although these uncertainties are independent, together they may give, in a worst-case situation of all bias in the same direction, an offset of 9.7 K. For independent errors added in quadrature (i.e., the square root of the sum of the squares) they give a mean offset of 5.8 K. Because the temperature offset based on these 11 nights of data ranges from −10 to +12 K, there may possibly be additional uncertainties in the HSRL system calibration. The spectral purity is not quantitatively known and can give larger offsets, but it should shift only the measured temperature profiles to higher values. However, offsets colder than the balloon measurements have been observed. A frequency shift (chirp) in the pulse laser output relative to the cw frequency used for laser locking could also create an offset. If the frequency shift was large (~40 MHz), the sensitivity would change and would therefore also affect the lapse rate of the temperature profiles. In any event, using a reference temperature at one range height and one time for the present system, we can determine the calibration constant (ξ_1/ξ_2) or $(\xi_1\xi_2'/\xi_2\xi_1')$ without the laboratory normalization measurement described in Section 3, and the temperature offset is eliminated. Therefore, for practical measurements with this lidar, a known reference temperature each night is needed for absolute measurement of the temperature profiles. With the additional reference input, the HSRL system provides a practical means for accurate (nearly photon-noise-limited) lidar temperature (thus pressure and density as well) measurements.

The sources for the measurement uncertainty include stability of frequency lock, iodine filter transmission, and PMT high voltage as well as photon noise. Again, each of these error sources and the corresponding uncertainties have been discussed in detail.[26] Here we comment only on the PMT (high-voltage) stability. Because we desire the highest linearity to increase the PMT count rate, the discriminator threshold must be set to give the best linearity over the dynamic range of the lidar signal; and, in our case, the stability of the PMT was compromised. This has been studied[26] and is not repeated here. For the PMT used, we found, not surprisingly, that the slope of the photon count rate is greatest for the chosen high-voltage set point for a maximum linear count rate. The fractional change in the counts for a 1-V (0.01 V in the control voltage) change in the high voltage is ~1.7%. Because the discriminator and supply voltage are set to give the best linearity, the options to improve the stability are to control the high voltage more accurately or compromise the maximum linear count rates.

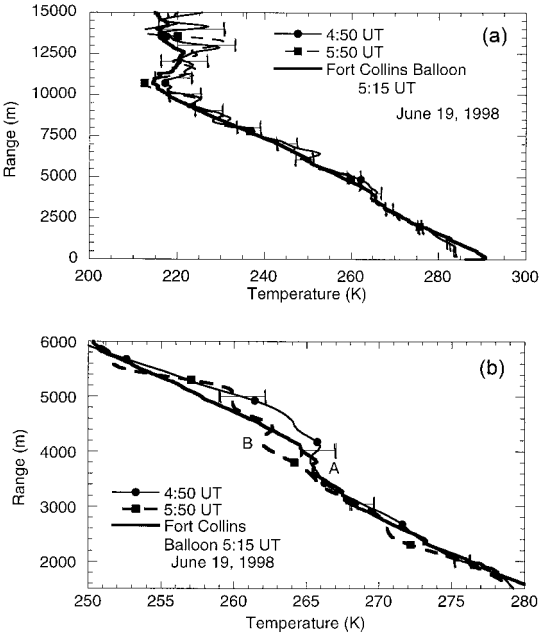

Fig. 9. (a) Sample HSRL 1-hr, 300-m averaged temperature profiles for 19 June, 1998 plotted with Fort Collins balloonsondes. The error bars give the photon-counting error at 1-km intervals for the first hourly HSRL profile. (b) Expanded plot of the inversion near 4 km; the altitude of the inversion moves up during the night from point A to point B.

The calibration and measurement error bars for the backscatter ratio were also analyzed in detail. Because of the difficulty in the measurement of the relative efficiency between total scattering and molecular-scattering channels, there exists a possible offset of a few percent as well (Table 2). The measurement errors were assessed to be 0.97% and 1.7%, respectively, at 5 and 10 km for the same resolution of 1 hr and 300 m.

C. Salient Features in Hourly Mean Profiles

Figure 9(a) shows sample hourly averaged temperature profiles for 19 June, 1998 with the same offset correction applied for all hours because the normalization value was found to be constant throughout the night. The tropopause altitude is observed in all the lidar profiles and agrees with the balloon data. The

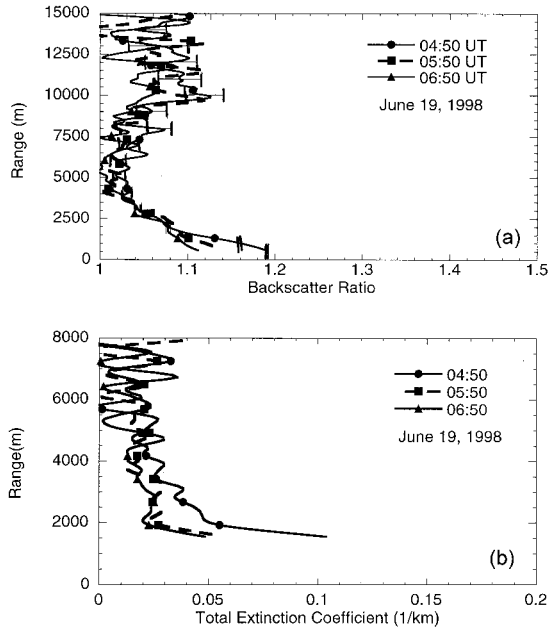

Fig. 10. (a) Sample HSRL 1-hr, 300-m averaged backscatter ratio profiles for 19 June, 1998. The error bars give the photon-counting error at 1-km intervals for the first hourly HSRL profile. (b) Sample HSRL 1-hr, 300-m averaged extinction coefficient profiles for 19 June, 1998.

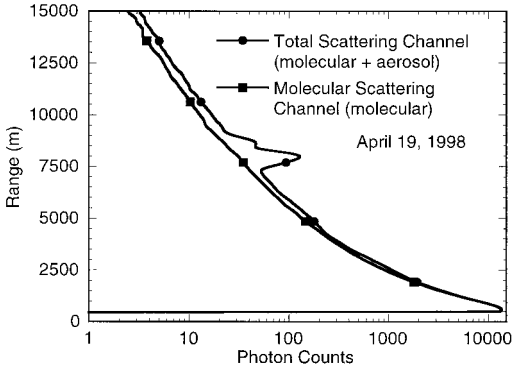

Fig. 11. Raw data profile averaged over 3 min and 300 m for one of the molecular-scattering channels and the total scattering channel for the night of 19 April, 1998. The total scattering channel shows a cloud at ~8 km.

uncertainty that is due to photon-counting statistics for these profiles is less than 1 K below 3.5 km. The data show a small temperature inversion at ~4 km, which is also evident in the Fort Collins balloon data. Because the temperature profile remained fairly constant, the range height (~4.2 km) of the temperature inversion is approximately the same for the HSRL and the balloon data, where an expanded plot of the hourly average temperature profiles near 4.2 km is shown in Fig. 9(b). The inversion range height moved up from point A at 4:50 UT to point B at 5:50 UT and remained there for four more hours (not shown). The 4:50 UT lidar profile agrees well with the 5:15 UT balloon data within the photon-counting errors. For each temperature profile, there are associated pressure and air density profiles, which together depict the state of the atmosphere as a function of height.

The hourly averaged backscatter ratios are shown in Fig. 10(a) with the photon-counting error shown for the first hour. The lower altitudes demonstrate a decrease in the backscatter ratio of nearly 10% over the course of the night. There was no significant cloud backscatter this night. The planetary boundary layer is evident from the backscatter ratios showing the altitude and magnitude of the backscattering decreasing during the night.

The total extinction coefficient profiles are shown in Fig. 10(b). As in the backscatter ratio profiles, the first hour (~2 hr before local midnight) shows significantly higher values in the planetary boundary layer. Because the efficiency factor ξ_i in Eq. (8) is z dependent at lower ranges because of the telescope overlap function, we truncated the extinction coefficient at 1000 km. The extinction coefficient is calculated from the derivative of the molecular-scattering channel, Eq. (8), which is greatly affected by the photon-counting uncertainties. Therefore the upper ends of the profiles in Fig. 10(b) were truncated at 8 km. Despite a small power-aperture product (0.19 Wm^2), this set of Figs. 9–10 clearly demonstrates the capability of HSRL for simultaneous measurement of atmospheric-state and aerosol optical parameters.

As Table 2 indicates, the data for 19 April, 1998 showed little or no temperature offset from the Denver balloon data. The photon count rate at the lower ranges was lower than those on 19 June, 1998 and showed no problem of nonlinearity in the photocounts resulting from a photon piling-up effect. A plot of photon counts in Fig. 11 shows how the shapes of the total scattering profile and the molecular-scattering profiles differ when a cloud is present. This shows that the iodine filters in the molecular channels are effective in removing the aerosol scattering.

The 2-hr mean-temperature profiles at 5:00, 7:00, and 9:00 UT in Figs. 12(a) and 12(b) are interesting both because of the presence of a cloud layer at ~7.6 km and because two Denver balloon soundings before and after the lidar profiles show differences. Fortunately, the two balloon temperatures at ~1.5–2.0 km agree, and they also agree with the lidar-measured temperature at that height. In general, the lidar temperatures between 1 and 7 km are in agreement with the balloon sounding taken at 0 UT, whereas the tropopause lidar temperatures are in agreement with the balloonsonde taken at 12 UT. Shown in the legend of Fig. 12 are also the calculated lapse rates for both the balloon and the lidar data from a linear fit between 1 and 7.5 km. The hourly mean backscatter ratio profiles are shown in Fig. 13. A cloud layer with a backscatter ratio of >3.5 can be seen at 7.6 km at 6 and 7 UT, yet the corresponding temperature profiles [Figs. 12(a) and 12(b)] show no abnormality. It should be pointed out that there are many 3-min profiles with backscatter ratios as high as 20 within the hour with a mean backscatter ratio of 3.5. By

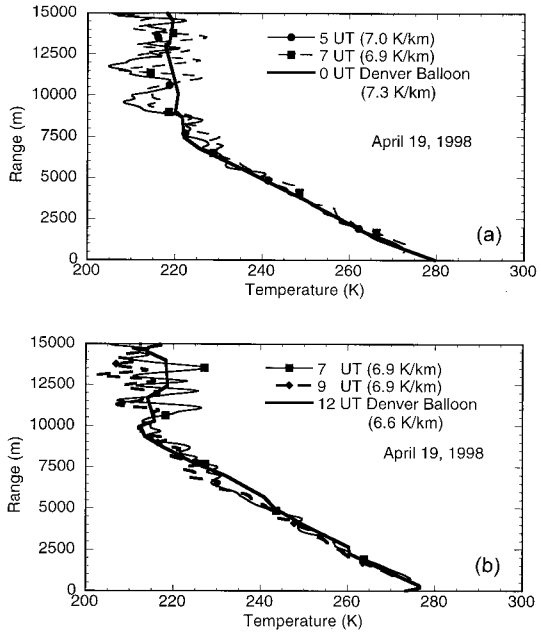

Fig. 12. (a) and (b) HSRL 2-hr, 300-m averaged temperature profiles for 19 April, 1998 plotted with Denver balloonsondes.

this example, we have shown that the iodine filters are effective in blocking aerosol scattering with a backscatter ratio as large as 20 and that the data obtained are adequate for the retrieval of temperature profiles. Although lidar temperatures for the night of 19 April agree with the results of balloon sounding without the need for adjustment, the backscatter ratio as plotted in Fig. 13 does show an offset of ~5% (Table 2). Without adjustment, the backscatter ratio is less than 1 for heights above 7.5 km. If desired, an adjustment in the relative efficiencies between the total and the molecular-scattering channels would improve the appearance of the backscatter ratio profiles shown.

6. Discussion

There are two general methods to retrieve atmospheric temperature profiles from lidar scattering signals. The first one (inversion technique) uses a successive integration of lidar return from different heights when we assume that the ratio of scattered intensities between two heights is equal to the ratio of atmospheric densities between the same two heights. Rayleigh lidar and vibrational Raman lidar typically use this technique to deduce atmospheric profiles. This technique may be problematic when a sharp gradient exists in the extinction profile as often encountered in the troposphere. The second one (ratio technique) spectrally filters the scattered signal into two different channels, and the ratio of the two filtered signals at the same range height provides a unique determination of atmospheric temperature at the given range height. Rotational Raman lidar and the HSRL discussed here use this technique for temperature retrieval. The advantage of the ratio technique is that it is immune from the vertical gradient in the extinction coefficient. However, a stable, relative efficiency is required because two channels are used. Unfortunately, all narrow-band optics, e.g., beam splitters, interference filter, and iodine filters in our case, intrinsically lack long-term stability at the present time. Periodic calibration may be necessary.

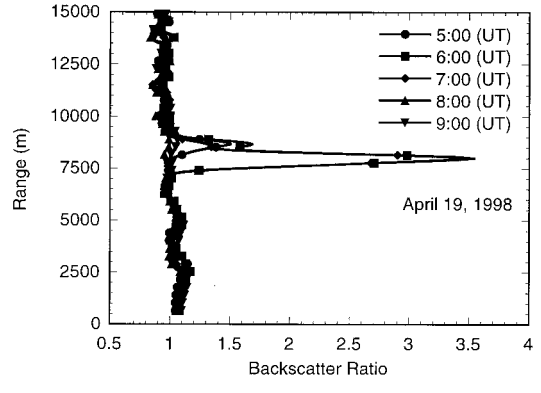

Fig. 13. HSRL 2-hr, 300-m averaged backscatter ratio profiles for 19 April, 1998.

The requirement of an adjustment by means of calibrating against a sounding temperature measurement at one height on a nightly basis is mainly due to the instability of the relative efficiency in the different channels and the changes in the frequency-independent transmission of the iodine filter. Although annoying, the difficulty of accurate efficiency measurement is well known and often requires calibration for its resolution in lidar data analysis and retrieval. For example, in rotational Raman lidar[11] a temperature profile on a nightly basis over the range of a balloon sounding is used to determine the two calibration constants in the measured intensity ratio in the form of $A + B/T$ because the narrow-band interference filters used in the receiver are temperature and humidity sensitive. Like the problem we experienced, the calibration constants A and B made on one night may not be valid for a different night. However, such a stability problem is not intrinsic; improvement is possible with technology. Indeed, with more stable interference filters of 0.002 nm/K, recently the GKSS rotational Raman lidar[12] needed only one calibration for the entire seasonal campaign.

In our HSRL at 589 nm, only one iodine filter was used. The temperature was determined from lidar returns at two preselected frequencies.[20] Because the efficiency and conditions of optical components are expected to remain the same within the time scale of a minute, the problem of relative efficiency becomes a nonissue. Indeed, with limited field experimentation, we did not notice any temperature offset problem in our 589-nm system.[20] Before a system with long-term stability is developed, it is also possible to operate the HSRL at 532 nm with use of only one vapor filter and one detector for temperature profiles. In this case, one locks the YAG laser at a frequency and uses a double-path acousto-optic modulator to move to a second or a third selected fre-

Table 5. Rough Signal Strength and Bandwidth Comparison for Different Scattering Lidars for Atmospheric Temperature Measurements

Lidar	Method	Relative Signal Strength	Signal Bandwidth Night (Day)	Comments
Rayleigh	Inversion	1	5 nm (100 GHz)	Must be aerosol free
HSRL 1	Ratio	0.2	10 GHz	Can handle aerosol
HSRL 2	Inversion	0.4	10 GHz	Cannot handle extinction gradient
Rotational Raman	Ratio	0.004	5 nm	Can handle aerosol
Vibrational Raman	Inversion	0.001	5 nm (100 GHz)	Cannot handle extinction gradient

quency. We developed the high-efficiency double-path acousto-optic modulator technique for fluorescence lidar applications[29,30]; it has been recently adopted for a different version of HSRL with doubled YAG lasers. Liu *et al.*[31] used an acousto-optic modulator to move the seeder for the double YAG laser between two frequencies, one in the absorption well of an iodine line and the other at its edge. The on-resonance signal is used to retrieve atmospheric temperatures by the inversion method, and the ratio of the two signals can be used to retrieve the backscatter ratio profile. As noted, the problem with the inversion method lies in its difficulty in the handling of the vertical gradient in the extinction coefficient. But the inversion method does not depend on a wide filter bandwidth to gain temperature measurement sensitivity. This is an advantage in that an iodine cell at a lower temperature, giving a relatively narrower notch filter, can be used. Because a lower-temperature cell will not suffer continuum absorption as much, it has a higher transmission for the Cabannes-scattering signal.

As mentioned above, an intrinsic problem with an iodine-vapor filter with a wide width is the continuum absorption. This broadband absorption depends on vapor density (thus temperature). The transmission of our hot filter is only 14% at an off-resonance frequency ν_0 and it transmits only 1% of the Cabannes signal on resonance. As such, the larger scattering cross section of Cabannes scattering is somewhat negated. To be more specific, we recall that, relative to Cabannes scattering, rotational Raman scattering is ~2.5%, and vibrational Raman scattering by nitrogen is ~0.1%. In the case of rotational Raman lidar, because of the need to gain temperature sensitivity, different spectral segments must be selected; only ~20% of the 2.5% is useful; for the same power-aperture product, a rotational Raman lidar has ~0.5% signal as compared with a Rayleigh lidar. The present HSRL at 532 nm with a 1% useful signal has only two times more signal than a rotational Raman lidar. To improve off-resonance transmission, we need a way to increase the absorption linewidth without increasing the continuum absorption. One way to do this is to use a cell with iodine mixed with an appropriate amount of rare gas, such as argon. At a given temperature, the collision broadening with argon atoms will broaden the iodine absorption line without changing the continuum absorption. In this manner, it is reasonable to expect the same sensitivity of 0.42%/K with, say, 20% transmission of the Cabannes signal through the hot cell, giving the HSRL 40 times more signal than that of a rotational Raman lidar. Using HSRL with the inversion technique, we can expect to transmit 40% of the Cabannes signal because a narrow absorption well is sufficient. Another advantage for HSRL is that the signal of interest is contained within ~10 GHz, so a narrow-band system can be used, making daytime implementation practical. To gain a qualitative perspective, we compare the signal strength and the bandwidth of various methods for temperature profiling in Table 5. A more extensive table comparing the strength and width of all scattering lidars known has just been published.[23]

It should be pointed out that the rejection of aerosol scattering is essential from atmospheric temperature measurements with a scattering lidar. Rayleigh lidar does this in an aerosol-free region. In the case of rotational and vibrational Raman lidars, in which the useful signal is at least 1 nm away from the elastic Mie scattering, interference filters can be used to reject aerosol scattering. Because the Mie scattering with a bandwidth of the order of tens of megahertz occurs at the center of the Cabannes-scattering spectrum, which is ~10 GHz wide, only atomic or molecular vapor notch filters can disentangle the Mie spectrum from the Cabannes spectrum better than a Fabry–Perot interferometer, which eliminates the Mie signal all together. Because the Cabannes-scattering spectrum is Doppler shifted by the line-of-sight wind, use of an iodine-vapor filter for wind measurements has been reported in the literature.[32,33]

7. Conclusion

We have presented an account of our development for a HSRL at 532 nm capable of measuring vertical profiles of atmospheric-state parameters (temperature, pressure, and density) and optical aerosol parameters (backscatter ratio and aerosol extinction coefficient). This is made possible by use of an iodine-vapor filter operating at a temperature that the absorption lines 1107 and 1108 overlap, leading to a high measurement sensitivity of 0.42%/K.

Although the power-aperture product of this working system is only 0.19 Wm^2, the HSRL can measure a temperature profile up to 15 km (resolution 300 m) with 1 hr of integration. The 1σ measurement uncertainties are 1.9 K (0.97%) and 2.4 K (1.7%) at 1

and 5 km, respectively, for temperatures (backscatter ratio). Because of a slow system instability that still exists, an additional adjustment on the relative efficiency between the two molecular channels is needed to obtain absolute temperatures with photon-noise-limited accuracy. In practice, we can provide the needed calibration constant by inputting temperature and pressure values at one range height and one time (by independent measurement from a collocated weather tower or perhaps by a tethered balloon) for one night of observation. Regardless of the offset, the lidar data show good agreement in the lapse rates, tropopause altitudes, and inversions in the temperature profile when compared with the result of balloon sounding. It is suggested that the detection system stability is not an intrinsic problem and it can be improved in the future.

With further improvements on the spectral purity of the transmitting laser source and the system stability, one can hope to eliminate the need for this additional calibration and approach the theoretical HSRL performance. Because the offset problem lies in the variation of relative efficiency between two channels, it may be possible to develop a frequency-agile system with a gigahertz acousto-optic modulator[29] so that the required molecular-scattering ratio for the determination of temperature can be obtained with one iodine filter. This approach, however, as in the 589-nm system, would necessarily reduce the lidar duty cycle by a factor of 2, reducing the signal-to-noise ratio of the measurement. Another problem that reduces the effective use of laser power is the continuum absorption that exists in iodine vapor under high operating temperatures.[25] Creative ways to increase the iodine absorption linewidth (by pressure broadening with buffer gas, for example) without an increase in the filter temperature should be explored. This will increase the signal level to be 40 times stronger than rotational Raman lidar and 200 times stronger than vibrational Raman lidar.

We acknowledge support in part through contract DAAHO4-94-G-0420 with the U.S. Army Center for Geoscience at Colorado State University. The balloon measurements at Fort Collins were made by John Davis from the Department of Atmospheric Science at Colorado State University.

References

1. G. Fiocco, G. Beneditti-Michelangeli, K. Maischberger, and E. Madonna, "Measurement of temperature and aerosol to molecule ratio in the troposphere by optical radar," Nature (London) Phys. Sci. **229,** 78–79 (1971).
2. A. T. Young, "Rayleigh scattering," Phys. Today **35,** 42–48 (1982).
3. R. L. Schwiesow and L. Lading, "Temperature profiling by Rayleigh-scattering lidar," Appl. Opt. **20,** 1972–1979 (1981).
4. L. Elterman, "Stratospheric temperature profiles obtained from searchlight measurements," Phys. Rev. **92,** 1080 (1953).
5. L. Elterman, "Seasonal trends of temperature, density, and pressure to 67.6 km obtained with the searchlight probing technique," J. Geophys. Res. **59,** 351–358 (1954).
6. G. S. Kent and R. W. H. Wright, "A review of laser radar measurements of atmospheric properties," J. Atmos. Terr. Phys. **32,** 917–943 (1970).
7. A. Hauchecorne and M. L. Chanin, "Density and temperature profiles obtained by lidar between 35 and 70 km," Geophys. Res. Lett. **7,** 565–568 (1980).
8. P. Keckhut, M. L. Chanin, and A. Hauchecorne, "Stratosphere temperature measurement using Raman lidar," Appl. Opt. **29,** 5182–5185 (1990).
9. J. Cooney, "Measurement of atmospheric temperature profiles by Raman backscatter," J. Appl. Meteorol. **11,** 108–112 (1972).
10. J. Cooney, "Atmospheric temperature measurement using a pure rotational Raman lidar: comment," Appl. Opt. **23,** 653–654 (1984).
11. N. Nedeljkovic, A. Hauchecorne, and M.-L. Chanin, "Rotational Raman lidar to measure the atmospheric temperature from the ground to 30 km," IEEE Trans. Geosci. Remote Sens. **31,** 90–101 (1993).
12. A. Behrendt and J. Reichardt, "Atmospheric temperature profiling in the presence of clouds with a pure rotational Raman lidar by use of an interference-filter-based polychromator," Appl. Opt. **39,** 1372–1378 (2000).
13. S. T. Shipley, D. H. Tracy, E. W. Eloranta, J. T. Tauger, J. T. Sroga, F. L. Roesler, and J. A. Weinman, "High spectral resolution lidar to measure optical scattering properties of atmospheric aerosols. 1: Theory and instrumentation," Appl. Opt. **22,** 3716–3724 (1983).
14. H. Shimizu, S. A. Lee, and C. Y. She, "High spectral resolution lidar system with atomic blocking filters for measuring atmospheric parameters," Appl. Opt. **22,** 1373–1381 (1983).
15. R. J. Alvarez II, L. M. Caldwell, Y. H. Li, D. A. Krueger, and C. Y. She, "High-spectral-resolution lidar measurement of tropospheric backscatter-ratio with barium atomic blocking filters," J. Atmos. Oceanic Technol. **7,** 876–881 (1990).
16. P. Piironen and E. W. Eloranta, "Demonstration of a high-spectral-resolution lidar based on an iodine absorption filter," Opt. Lett. **19,** 234–236 (1994).
17. E. Voss, C. Weitkamp, and W. Michaelis, "Lead-vapor filters for high-spectral-resolution temperature lidar," Appl. Opt. **33,** 3250–3260 (1994).
18. C. Y. She, R. J. Alvarez II, L. M. Caldwell, and D. A. Krueger, "High-spectral-resolution Rayleigh–Mie lidar measurement of aerosol and atmospheric profiles," Opt. Lett. **17,** 541–543 (1992).
19. R. J. Alvarez II, L. M. Caldwell, P. G. Wolyn, D. A. Krueger, T. B. McKee, and C. Y. She, "Profiling temperature, pressure, and aerosol properties using a high spectral resolution lidar employing atomic blocking filters," J. Atmos. Oceanic Technol. **10,** 546–556 (1993).
20. L. M. Caldwell, "A high spectral resolution lidar using an iodine vapor filter at 589 nm," Ph.D. dissertation (Department of Physics, Colorado State University, Fort Collins, Colo., 1994).
21. M. D. Levenson and A. L. Schawlow, "Hyperfine interactions in molecular iodine," Phys. Rev. A **6,** 946–951 (1972).
22. A. Arie, S. Schiller, E. K. Gustafson, and R. L. Byer, "Absolute frequency stabilization of diode-laser-pumped Nd:YAG lasers to hyperfine transitions in molecular iodine," Opt. Lett. **17,** 1204–1206 (1992).
23. C. Y. She, "Spectral structure of laser light scattering revisited: bandwidths of nonresonant scattering lidars," Appl. Opt. (In press). LP17498.
24. D. A. Krueger, L. M. Caldwell, R. J. Alvarez II, and C. Y. She, "Self-consistent method for determining vertical profiles of aerosol and atmospheric properties using a high spectral resolution Rayleigh-Mie lidar," J. Atmos. Oceanic Technol. **10,** 534–545 (1993).
25. J. W. Hair, "A high spectral resolution lidar at 532 nm for simultaneous measurement of atmospheric state and aerosol

profiles using iodine vapor filters," Ph.D. dissertation (Department of Physics, Colorado State University, Fort Collins, Colo., 1998).
26. G. Tenti, C. D. Boley, and R. C. Desai, "On the kinetic model description of Rayleigh-Brillouin scattering from molecular gases," Can. J. Phys. **52,** 285–290 (1974).
27. J. Tellinghuisen, "Transition strengths in the visible-infared absorption spectrum of I_2," J. Chem. Phys. **76,** 2821–2834 (1982).
28. J. N. Forkey, "Development and demonstration of filtered Rayleigh scattering—a laser based flow diagnostic for planar measurement of velocity, temperature and pressure," Ph.D. dissertation (Department of Mechanical and Aerospace Engineering, Princeton University, Princeton, N.J., 1996).
29. C. Y. She and J. R. Yu, "Simultaneous 3-frequency Na lidar measurements of radial wind and temperature in the mesopause region," Geophys. Res. Lett. **21,** 1771–1774 (1994).
30. M. A. White, D. A. Golias, D. A. Krueger, and C. Y. She, "Frequency-agile lidar for simultaneous measurement of temperature and radial wind in the mesopause region without sodium density contamination," in *Application of Lidar to Current Atmospheric Topics*, A. J. Sedlacek, ed., Proc. SPIE **2833,** 136–140 (1996).
31. Z. Liu, I. Matsui, and N. Sugimoto, "High-spectral-resolution lidar using an iodine absorption filter for atmospheric measurements," Opt. Eng. **38,** 1661–1670 (1999).
32. Z. S. Liu, W. B. Chen, T. L. Zhang, J. W. Hair, and C. Y. She, "An incoherent Doppler lidar for ground-based atmospheric wind profiling," Appl. Phys. B **46,** 561–566 (1997).
33. J. S. Friedman, C. A. Tepley, P. A. Castleberg, and H. Roe, "Middle-atmosphere Doppler lidar using an iodine-vapor edge filter," Opt. Lett. **22,** 1648–1650 (1997).